Title
SINGLE PHOTOELECTRON TIME SPREAD MEASUREMENT OF FAST PHOTOMULTIPLIERS

Authors
Leskovar, Branko
Lo, C.C.

Publication Date
1974-07-01

Presented at the International Conference on
Precision Electromagnetic Measurements,
London, England, July 1-5, 1974.

LBL-3063
c.1

SINGLE PHOTOELECTRON TIME SPREAD MEASUREMENT OF FAST PHOTOMULTIPLIERS

Branko Leskovar and C. C. Lo

July 1, 1974

Prepared for the U. S. Atomic Energy Commission
under Contract W-7405-ENG-48

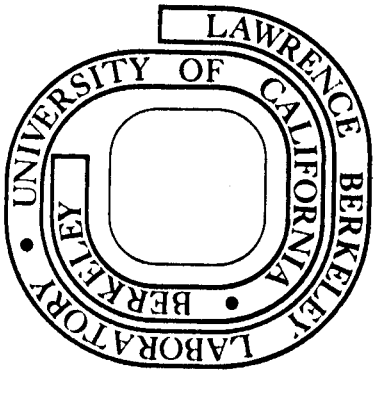

LBL-3063
c.1

DISCLAIMER

LBL-3063

Single Photoelectron Time Spread Measurement of Fast Photomultipliers

Branko Leskovar, C. C. Lo
Lawrence Berkeley Laboratory
University of California
Berkeley, California

Abstract

Time spread measurements, using single photoelectrons of fast photomultipliers having dynodes with cesium-activated gallium-phosphide secondary emitting surfaces have been investigated. Measurements of the time spread, made by means of a specially developed measuring system with improved time resolution capabilities, on several 8850's and C31024's are presented and discussed. Critical evaluation of the measuring system is given, particularly concerning the influences of the light pulse width and the constant fraction discriminator timing errors on the system time-resolution capabilities. The measuring system incorporates a subnanosecond light-pulse generator capable of operating at a repetition rate of 3 MHz with output light pulses having a full width at half-maximum of less than 200 psec. It also incorporates a constant fraction

discriminator which has a time walk less than ±35 psec over a range of input-pulse amplitudes from 35mV to 8V. The optimum operating conditions of the photomultipliers have been determined for minimum time spread and relative collection efficiency. The error of the time spread measurements, because of the finite width of the light pulse, is discussed and determined for different pulse widths.

Introduction

Fast electrooptical devices, such as standard and microchannel photomultipliers and electron multipliers, offer the most sensitive and accurate means for recording the collision of a photon, electron, atom, or energetic ion with a target surface. Consequently, these devices have gained wide acceptance in experimental research, particularly in mass spectroscopy [1] and scintillation spectrometry [2]. Generally, the detection process begins at the photocathode, where primary photons produce photoelectrons, or at the dynode, where a primary particle produces secondary electrons. Charge multiplication of photoelectrons or secondary electrons involves generation of secondary electron cascades between dynodes in vacuum. Because of the statistical variations inherent in the conversion of photons to photoelectrons, and the statistical nature of the secondary emission process, the output signal

varies from one pulse to the next, even for an equal number of incident photons or primary particles. Consequently, the resulting distribution in output pulse heights limits not only the resolution, but may also affect the time resolution.

The investigation of time-resolution capabilities is becoming increasingly important in a multitude of research areas, such as atomic and molecular subnanosecond fluorescence decay time measurements, [3], nuclear research instrumentation [4], optical ranging experiments, [5], optical communication [6], and photon statistics experiments [7]. In this paper the time capabilities of fast standard and microchannel type photomultipliers are of particular interest. Resolution capabilities in this case are essentially determined by the random deviations in the transit time of electrons traveling from photocathode to collector.

The electron transit time spread is mainly caused by fluctuations of individual times of flight of photoelectrons and secondary electrons due to their different trajectories and their initial velocity differences. The factors that contribute to the transit time spread are differences in trajectory length and in electrical field strength for different portions of the photocathode-first dynode region, and between various dynode sections. Generally, the amount of transit time spread depends upon photomultiplier geometric

characteristics, its operating conditions, and the number of photoelectrons released from the photocathode. Since the time spread varies approximately inversely as the square root of the number of photoelectrons, the time behavior information of single photoelectrons is particularly helpful in predicting the transit time spread for an arbitrary number of photoelectrons. Furthermore, it is also helpful in the evaluation, selection and comparison of photomultipliers, as well as in determination of photomultiplier optimum operating conditions in critical applications. This is particularly important in areas of experimental research where single photoelectron detection and precise subnanosecond timing are required, and where timing capabilities of a photomultiplier are the limitation to the precision of a measurement, [8]. Consequently, the best characterization of the photomultiplier electron transit time spread is given by the single photoelectron time performance.

Measurements of photomultiplier characteristics, including the single photoelectron time spread, have previously been done for fast photomultipliers having dynodes with conventional secondary emitting surfaces [9], and for photomultipliers having dynodes with cesium-activated gallium-phosphide secondary emitting surfaces, [10]-[14]. Also, a special measuring system has been

developed for studying and optimizing the time resolution capabilities of fast standard and microchannel type photomultipliers, [15]. However, our measurements have shown that contemporary fast high-gain photomultipliers have so small a time spread that the rise time and the width of the light pulse, as well as discriminator timing errors, have significant influence on measured results with single photoelectrons. Furthermore, a critical evaluation of the measuring system has shown that the full width at half maximum of the light pulse presents a serious limitation to the time resolution that can be measured. Therefore, an improved measuring system has been developed with better system time resolution than previously available. With the improved system, a study has been made of the performance of contemporary photomultipliers having GaP(Cs) dynodes and the ways of optimizing this time performance.

Electron Transit Time Spread Considerations

The total electron transit time spread of an electrostatically focused photomultiplier consists of the photoelectron transit time spread between the photocathode and the first dynode of the multiplier, the electron transit time spread in the electron multiplier, and that between the electron multiplier and the anode. The major causes of transit time spreads are the distribution of initial emission velocities of photoelectrons and secondary

electrons, unequal electron path lengths between different electrodes and nonuniform electric fields. Generally, the initial stages of a photomultiplier contribute with the greatest weight to the total transit time spread. In the latter stages, the larger number of electrons in the pulse provide many samples of transit time through the stage and reduce the transit time spread of that stage in the manner of the standard error of mean value. The variance of the total single photoelectron transit time, t_σ^2 , is approximately given by the following equation [16]:

$$t_\sigma^2 \approx t_{CD1}^2 + \frac{t_{D1D2}^2}{g_1}(1 + g_{\sigma 1}^2) + \frac{t_{DD}^2}{g_1(g-1)}(1 + g_\sigma^2) \qquad (1)$$

where t_{CD1}^2 is the variance of the photoelectron transit time between the photocathode and the first dynode, t_{D1D2}^2 is the variance of the electron transit time between the first and the second dynode, t_{DD}^2 is the variance of the electron transit time between two successive dynodes, g_1 is the gain of the first dynode, g is the gain of all other dynodes, $g_{\sigma 1}^2$ is the variance of the gain g_1, and g_σ^2 is the variance of the gain g.

The relation (1) shows that the total transit time variance will be considerably reduced using dynodes with emitting surfaces that have a high and uniform secondary emission yield. The total single photoelectron transit

time spread, expressed by the full width at half maximum, is related to the standard deviation of the total transit time by the expression:

$$t_{\sigma FWHM} \approx 2.36\ t_{\sigma} \tag{2}$$

The contribution to the transit time spread by the unequal electron path lengths between different electrodes and the nonuniformity of electric fields at the dynodes can be minimized by proper design of the input electron optics and the electron multiplier. This has been one of the goals of the photomultiplier manufacturers. Therefore, the ultimate limitation on time spread is determined by initial velocity effects of photoelectrons and secondary electrons. Assuming a uniform electric field between the photocathode and the first dynode, and equal photocathode to first dynode electron path lengths, the time spread between a photoelectron emitted with zero initial velocity and a photoelectron with velocity v_o is approximately given by the equation, [17]

$$\Delta t_n \approx \frac{v_o \ell}{eV}\ m_o \tag{3}$$

where ℓ is the distance between the photocathode and the first dynode, V is the voltage between the photocathode and the first dynode, and e and m_o are the charge and mass of an electron, respectively.

It can be seen from this equation that transit time spread resulting from the initial velocity distribution is decreased by increasing the voltage between the photocathode and the first dynode. Similar considerations are valid for the secondary electron initial velocity in an electron multiplier.

The single photoelectron time spread and time response of photomultipliers have improved considerably within the last few years, due both to better electron optical design and to the application of new secondary emitters. Secondary emission limitations, which result from the short escape depth of electrons in conventional secondary emitters, are reduced substantially by the use of cesium-activated gallium-phosphide secondary emitters. In these emitters a reduction of the surface barrier and the bending of energy bands occur when the electropositive cesium is deposited on heavily doped p-type crystals of gallium phosphide [18]. Under these conditions, electron affinity is smaller than the band gap of GaP. Electrons can pass through the bend-band region with a small loss of energy, and they can escape from distances at least an order of magnitude greater than those in conventional secondary emitters. Therefore, such a configuration behaves as if it has a negative electron affinity and consequently has a high secondary emission yield.

Secondary emission yields of GaP(Cs) surfaces are considerably higher, typically between 30 and 50 at a primary electron energy of 600 eV, than those obtained with conventional dynode materials, where average dynode gains of 5 to 8 can be achieved [19], [20]. Due to the higher secondary emission yield, photomultiplier electron multipliers require a fewer numbers of dynode stages than conventional electron multipliers for the same gain.

Computer simulation of the time broadening effect on an electron pulse in an electrostatically-focused photomultiplier shows that each dynode broadens the electron pulse as it passes through the multiplier structure [21]. Consequently, a smaller number of dynodes results in less time broadening and hence a faster time response of the photomultiplier.

Single photoelectron time spread is reduced in photomultipliers having dynodes with GaP(Cs) secondary emitting surface, in comparison with conventional dynode emitter photomultipliers, because of the higher gain of individual dynodes in the multiplier structure and the reduced influence of the electron initial velocity differences. The larger number of emitted secondary electrons from the first and second dynode reduces the electron transit time spread between the first dynode and the second dynode, as well as between the second and the third dynode.

As a result, more possible electron paths are sampled in each pulse, and time spread caused by geometrical path considerations is reduced. Furthermore, secondary electrons from GaP(Cs) dynodes have a smaller spread in initial velocity, in comparison with conventional emitters. The remaining electron initial velocity differences are reduced by employing a high potential gradient at the emitting surface. In this case the electrons are more quickly accelerated to their terminal velocity, and initial electron velocity has a reduced influence on the total transit time and its spread. The practical limit for a maximum value of interstage potential differences is determined by field emission from the elements and electroluminescence of insulating materials. Both of these processes can increase the amount of the photomultiplier dark current to an unacceptable level.

Block Diagram of Measuring System

The measurements of the single photoelectron transit time spread and of the relative collection efficiency were done by the system shown in Fig. 1. The system consists of a subnanosecond light pulse generator, a constant-fraction discriminator, leading edge discriminators, delay cables, a time-to-pulse amplitude converter, a multichannel analyzer, a pulse shaper, and a counter.

A reverse-biased electroluminescent diode, Ferranti type XP-23, driven by an avalanche transistor pulse generator, was used as the source of accurately timed, subnanosecond light pulses. It was shown in an earlier published work [15] that under reverse-biased conditions the XP-23 diode is capable of producing clean light pulses which have a full width at half maximum of less than 200 psec. The electroluminescent diode-photomultiplier spectra matching factors for RCA photomultipliers 8850 and C31024, having a bialkali photocathode, were calculated to be 0.050 and 0.052, respectively. The reverse-biased electroluminescence in the XP-23 diode was associated with avalanche breakdown, giving a clean subnanosecond light pulse with extremely short rise and decay time. This is due to the fact that the time constant for buildup of an avalanche process is extremely small, depending primarily upon carrier scattering time. When the current pulse is turned off, the built-in junction field sweeps the carrier into the n- and p-region. There they are the majority carrier and cannot give rise to radiative recombination. Consequently, it can be conclusively said that the full width at half maximum of the emitted light pulse is closely equal to the full width at half maximum of the diode current pulse. The electroluminescent diode required a current pulse of -1.33A

having a width at FWHM of 200 psec. The voltage across the diode was -20V. The diode breakdown voltage was approximately 10V at a temperature of 300°K.

The circuit designed to provide the operating subnanosecond current pulses for the diode consists of an avalanche transistor pulse generator and a step recovery diode pulse-shaping unit to steepen the front edge of the electrical pulse. A separate standard type pulse generator, capable of supplying pulses with nanosecond risetimes and amplitudes between 1V and 5V, was required to operate the subnanosecond current-pulse generator. The subnanosecond light pulse generator was capable of operating at a repetition frequency of 3MHz. The high repetition frequency is particularly desirable, since it shortens the measuring time necessary to obtain the required statistics for studying the single photoelectron time spread.

The light level of the subnanosecond light pulse generator was adjusted to a low intensity necessary to cause the emission of predominantly single-photoelectron levels by means of an optical attenuator. The photomultiplier single photoelectron time spread measurements were made with a small 1.6 mm diameter photocathode area and also with full photocathode illumination. For measurements with the 1.6 mm diameter area of photocathode

illumination, a positioning disc with a 3.2 mm hole in the middle was attached to the photomultiplier window. Sub-nanosecond light pulses were guided to the photocathode by means of a 12-inch long American Optical LG3 light guide to prevent the electromagnetic field of the light pulser from interfering with photomultiplier operation. For the measurements with full photocathode illumination, the positioning disc was removed. For measurements of photomultiplier C31024 transit time spread, an auxiliary anode bias supply, a variable attenuator, and two wideband amplifiers, Hewlett Packard Type 8447F, were inserted at points a and b. The auxiliary anode bias supply was necessary to obtain linear anode pulse currents of approximately 75mA peak from the C31024 [17]. The photomultiplier output pulses were processed in a specially designed constant-fraction discriminator, which has a time walk less than ±35 psec over a 35mV to 8V input-pulse amplitude variation. Since the measuring system time resolution depends almost entirely upon the constant-fraction discriminator time walk, the discriminator will be described later in this paper in considerable detail. The constant-fraction discriminator output was applied to a time-to-height converter via a discriminator-pulse shaper. The reference time pulse was obtained from the light pulser

and was passed through a delay line and a discriminator. The discriminator was followed by the time-to-height converter, whose output pulses were applied to a 400-channel pulse-height analyzer. For the relative collection efficiency measurements, the pulse shaper and counter were used to register the number of output pulses from the multichannel analyzer.

During measurements, the 30 nsec range of the time-to-pulse height converter was used. The converter registered the photomultiplier dark-noise pulses that were in coincidence with signal pulses within this range. The registered dark-noise pulse rate allowed by this gating operation was approximately 3×10^{-3} of the ungated noise rate in a worse case. The factor 3×10^{-3} is the fractional time when the photomultiplier channel was effectively open.

Measurements of Single Photoelectron Time Spread and Relative Collection Efficiency

In measuring the single photoelectron time spread the photocathode was exposed to subnanosecond light pulses from the light pulse generator of such low intensity that most of the light pulses produced no photoelectrons. In this case and for a given light pulse, the probability of producing n photoelectrons is approximately given by the Poisson distribution: $P(n) = m^n \exp(-m)/n!$, where m is the

expected number of photoelectrons per light pulse, and P(n) is the probability of obtaining n photoelectrons in a single light pulse. For values of m considerably below unity, $P(1) \approx m$, and the probability of producing more than a single photoelectron per light pulse is very small. Before the measurement, the ratio of the number of one-photoelectron events to two-photoelectron events was monitored with the pulse-height multichannel analyzer. Generally, a contamination of the single-photoelectron spectrum by multiple-photoelectron pulses was less than 1%. The difference between the time of arrival of a photomultiplier anode pulse resulting from a single photoelectron and the time of the reference pulse was measured, displayed, and recorded for a large number of light pulses. The single-photoelectron time spread of each of the spectra was calculated from the printout data, using the full width at half maximum (FWHM) points. The time spread was measured for 1.6 mm diameter area and also full photocathode illuminations. Generally, the amount of the single photoelectron time spread varies with the potential distribution in the input electron optics and the value of the supply voltage between the photomultiplier anode and cathode. The single photoelectron time spread was measured as a function of the voltage ratio between the photocathode-

focusing electrode and photocathode-first dynode, $(V_C-V_{FE})/(V_C-V_{D1})$, to determine the optimum photomultiplier operating conditions for minimum time spread. The supply voltage between the photomultiplier anode and cathode was taken as a parameter. The results of measurements for the RCA 8850 are given in Figs. 2 and 3, both for a 1.6 mm-diameter area and for full photocathode illumination, respectively. Measurements were made using the voltage divider network suggested by the photomultiplier manufacturer. The solid curves represent the typical single photoelectron time spread, FWHM, obtained by averaging the data for the four photomultipliers evaluated.

The relative collection efficiency was also measured during the optimization of the single photoelectron time spread, using the same measuring system. The relative collection efficiency is defined as the ratio between the efficiency of counting light pulses at any input electron lens potential and the efficiency of counting light pulses at optimum potential of the input electron optics. The collection efficiency varies with the potential distribution in the input electron optics and its value can be optimized for some photomultipliers. However, a potential distribution which maximizes relative collection efficiency does not necessarily minimize the single photoelectron time

spread. To determine the optimum photomultiplier operating conditions, the relative collection was measured as a function of the voltage ratio between the photocathode-focusing electrode and photocathode-first dynode, with the supply voltage between the cathode and anode as a parameter. Using the pulse shaper and counter to register the number of output pulses from the multichannel analyzer, the count rate was measured as a function of the $(V_C-V_{FE})/(V_C-V_{D1})$ ratio. The maximum amount of the count rate was used as the 100% relative collection efficiency point. The results of measurements for the RCA 8850 are given by dashed-line curves in Figs. 2 and 3, for 1.6 mm-diameter area and full photocathode area, respectively. For the C31024 the results of measurements are given in Figs. 4 and 5.

It can be seen from Fig. 2, that in the case of a 1.6 mm-diameter area of photocathode illumination at the center of the photocathode, the single photoelectron time spread has a minimum value, FWHM, of 0.33 nsec for $(V_C-V_{FE})/(V_C-V_{D1}) = 0.9$ and a supply voltage between anode and cathode of 3000V. Furthermore, the relative collection efficiency is 99% for the optimized value of single electron time spread. Consequently, in this particular case, the single photoelectron time spread can be easily optimized, almost without significant deterioration of the conditions

for maximum collection efficiency. Also, there is considerable decrease in the amount of the time spread when the anode supply voltage is increased from 2000V to 3000V, as has been explained in the previous section.

Similarly, with full photocathode illumination of 8850, the transit time spread has a minimum value FWHM of 0.48 nsec for $(V_C-V_{FE})/(V_C-V_{D1})$ = 0.95, and a supply voltage between the cathode and anode of 3000V.

The minimums of the time spread curves when the full photocathode is illuminated have higher values in comparison with the case of a 1.6 mm-diameter area of photocathode illumination, as might be expected because of the difference in transit time between the photoelectrons leaving the center of the photocathode and the photoelectrons leaving the photocathode from some other point. In the case of full photocathode illumination, single photoelectrons can be emitted from any point on the photocathode, thus contributing to the greater single-photoelectron time spread. Also, the minimums of the transit time spread curves are not as sharp as in the case of the 1.6 mm-diameter area of photocathode illumination, and they are closer to the $(V_C-V_{FE})/(V_C-V_{D1})$ = 1 point.

Maximum collection efficiency was obtained when $(V_C-V_{FE})/(V_C-V_{D1}) = 1.0$. The strong dependence of the amount of the time spread upon the value of the supply voltage is also evident. For example, at places where the curves have minimums, the time spread value is reduced from 0.63 psec to 0.48 psec if the supply voltage is increased from 2000V to 3000V.

Finally, the single-electron time spread for a particular 8850 with a 1.6 mm-diameter area of photocathode illumination and optimized $(V_C-V_{FE})/(V_C-V_{D1}) = 0.9$ ratio, as obtained on the display section of the multichannel analyser, is shown in Fig. 4.

The results of time spread measurements for the RCA C31024 are shown in Figs. 5 and 6 for a 1.6 mm-diameter area and also for full photocathode illumination. Measurements were made using a voltage divider network which was modified from the original divider suggested by the photomultiplier manufacturer. The modified divider gives considerably higher photocathode -- first dynode voltage,(i.e., 1100V at 4000V between the anode and cathode), compared with the original divider, (i.e., 660V at 4000V between the anode and cathode), resulting in a substantial decrease in the value of the single photoelectron time spread. As was the case for the

8850 measurements, the solid curves represent the typical single-photoelectron time spread, FWHM, obtained by averaging data for four photomultipliers. The results of the relative collection efficiency measurements are given in Figs. 5 and 6 by dashed-line curves.

In the case of the 1.6 mm-diameter area illumination at the center of the photocathode, the single photoelectron time spread has a minimum value, FWHM, of 0.3 nsec for $(V_C-V_{FE})/(V_C-V_{D1}) = 0.85$ and a supply voltage between anode and cathode of 4000V. Furthermore, the relative collection efficiency is 93% for the optimized value of the single-photoelectron time spread. For a supply voltage of 3000V, the collection efficiency is 99%. Again, the time spread can be easily optimized by changing the potential of the input electron optics, without seriously deteriorating the collection efficiency. Furthermore, there is a considerable decrease in the time spread value when the supply voltage between the anode and cathode is increased from 3000V to 4000V.

For the full photocathode illumination, the transit time spread has a minimum value of 0.42 nsec for $(V_C-V_{FE})/(V_C-V_{D1}) = 0.8$ and a supply voltage between the anode and cathode of 4000V. The value for the collection efficiency is 94%. The collection efficiency has a higher value, of 98%, for a supply voltage of 3000V. The minimum

of the time spread curves has a higher value, in comparison with a 1.6 mm-diameter area of photocathode illumination, due to the different values of transit time for photoelectrons emitted from the center of the photocathode and those emitted from some other point of the photocathode.

Finally, the single-photoelectron time spread for a particular C31024 with a 1.6 mm-diameter area of photocathode illumination is shown in Fig. 7, as obtained with the optimized ratio $(V_C-V_{FE})/(V_C-V_{D1}) = 0.85$ and $V_C-V_{D1}= 1100V$, on the display section of the multichannel analyzer.

In general, the behavior of the single-photoelectron transit time spread, and the relative collection efficiency shown in Figs. 2, 3, 5, and 6, should be considered as typical for types 8850 and C31024 photomultipliers. Since the average data were presented for four photomultipliers of each type, maximum absolute variations of ±8% for the position of the curve minimum along the $(V_C-V_{FE})/(V_C-V_{D1})$ axis of a particular photomultiplier can be expected from the averaged data. Concerning the value of the time spread, the maximum absolute variations are smaller than ±10% from the averaged data.

Although, in most cases where 8850 and C31024 photomultipliers are used, the operating conditions can be optimized for a minimum time spread without a significant

reduction in the relative collection efficiency value, it is suggested that for critical applications the optimization of the photomultiplier operating conditions should be done individually, following the method described above.

All previous considerations are based on the measured values of the single-photoelectron transit time spread. However, due to the finite width of the light pulse and its influence on the measured results, the measured values of the time spread are always larger than the true value of time spread in a fast photomultiplier, particularly when photomultiplier operating conditions are optimized for the minimum time spread. Consequently, it is important to estimate the error of the time spread measurements because of the finite width of the light pulse.

Influence of Finite Width of Light Pulse on Single Photoelectron Time Spread Measurements

Modern high gain, fast photomultipliers have so small a value of the single-electron time spread that, in addition to the time walk and resolution characteristics of the timing discriminator of the measuring system, the finite width of the light pulse has significant influence on the measured results. As a matter of fact, the full width at half maximum of the light pulse presents a fundamental limitation of the measuring system time resolution. For an accurate measurement of time spread, the width of the

light pulse should be as small as possible in comparison with the value of the electron time spread. If this is not the case, the light-pulse width will contribute directly to the amount of the electron time spread, due to the fact that photoelectrons can be emitted at any time during the existence of the light pulse. Because of the small value of time spread of contemporary photomultipliers, particularly where operating conditions are optimized for a minimum time spread, light pulse widths from conventional sources are, in most cases, comparable to the device time spread. An exception is the application of a mode locked Nd:glass laser in the measuring system. The laser can generate ultrashort light pulses with widths smaller than 6 psec in a pulse train. Single picosecond pulses can be selected from the pulse train with an electrooptical shutter. The pulse trains typically yield pulses too close together and too variable in amplitude to be used conveniently in the transit time spread measuring systems. Furthermore, the pulse generation typically occurs at a very low repetition rate. The highest repetition rate presently reported is 5 pulses per second, [23], [24]. Consequently, the application of a picosecond laser light pulser in the time spread measuring system is a complex, expensive, and relatively time consuming method, in comparison with presently available electroluminescent diodes. However, the laser application

in the measuring system is absolutely necessary when device transit-time spread measurements of ultimate accuracy are required, and when new, highly efficient photo- and secondary emitters with a longer electron emission time are explored.

Since, in most measuring systems for transit-time spread investigation, the electroluminescent diode is presently used as a source of subnanosecond light pulses, the dependence of measured values of device time spread upon finite width of the light pulse has been investigated in detail. Using a photomultiplier with optimized operating conditions for minimum single-photoelectron time spread, the time measurements were made as a function of width of the electroluminescent diode current pulse, with the supply voltage between the anode and cathode as a parameter. The results of measurements for the type 8850 are given in Figs. 8 and 9 for a 1.6 mm-diameter area and for full photocathode illumination, respectively. The curves represent the typical time spread, FWHM, obtained by averaging the data for four photomultipliers. During the measurements, an electroluminescent diode current pulse 200 psec wide was supplied by an avalanche transistor pulse generator in conjunction with a step recovery diode pulse-shaping unit. Electrical current pulses longer than 200 psec were obtained by means of a modified Tektronix 110 pulse generator. The width of the diode current pulse was

determined by a charging line. The diode current was monitored by using a Tektronix P6034 probe connected across a current shunt in series with the diode. The smallest width of the diode current pulse, expressed by FWHM, was 200 psec. For smaller widths than 200 psec the single-electron time spread curves were extrapolated to the 0.1 nsec point from experimental data obtained at larger diode current widths.

It can be seen from Figs. 8 and 9 that the single-electron time spread is a monotonically increasing function of the electroluminescent diode current pulse width. In the case where the diode current pulse width is considerably shorter than the photomultiplier single-electron time spread, as for example when the supply voltage between the anode and cathode is 2000V, the time spread curves show practically no dependence upon the current pulse width. Consequently, the measured value of the single-photoelectron transit time spread is practically equal to the true value of the time spread. Extrapolation shows that the error between the measured and the true value, taken at the 100 psec pulse current point, is approximately +6%, for a current pulse width of 200 psec. If the current pulse width equals 600 psec, a typical value in measuring systems for transit time spread previously used by some researchers, the error between the measured and true value of the time spread is +26%. When the diode pulse width is 1 nsec, the error

is +106%. For diode pulse widths larger than 2 nsec, the measured time spread, FWHM, is approximately equal to the FWHM width of the diode current pulse. Consequently, when the diode pulse current width is considerably larger than the single-electron time spread, the measured value of the single electron time spread is, in fact, closely equal to the width of the current pulse, and the difference between the measured and true values of the time spread is enormous. As a matter of fact, under these conditions, the time-correlated single-photoelectron counting technique was successfully applied to measure the decay times of plastic scintillators, [2] and in nanosecond fluorescence spectroscopy of macromolecules, [3], because the light pulse shape is statistically sampled by the single photoelectrons.

Generally, if the photomultiplier transit-time spread is considerably smaller than the width of the measured light pulse, the measured distribution is very closely equal to the wave shape of the light pulse. Under these conditions, the measured emission probability of photoelectrons is proportional to the light intensity. Also, measurement error increases as photomultiplier time spread decreases, for a constant value of the current pulse width, as can be seen from Figs. 8 and 9, for supply voltages between the anode and cathode of 2500V and 3000V. For example, it can be seen from Fig. 8 that for a supply

voltage of 3000V, the extrapolation, taken at the 100 psec pulse current width, shows an error between the measured and true time spread values of approximately +14%, at a pulse width of 200 psec. In such cases, the accuracy of the extrapolation to obtain the true value of the time spread is also decreased. It is assumed in these considerations that the light pulse shape closely follows the diode current pulse shape.

Similar measurements were performed for photomultiplier C31024. The results are shown in Figs. 10 and 11, for a 1.6 mm-diameter area and for full photocathode illumination, respectively. As in the previous case, the curves represent typical time spread FWHM, obtained by averaging the data for four multipliers. From the figures, and from a comparison with data which have been obtained for the type 8850, it can be seen that the finite width of the diode current pulse has a greater influence on the time spread true value than for the 8850 photomultiplier.

It can be seen from the figures and from comparison with the data obtained for the 8850 photomultiplier, that the finite width of the current pulse has a larger influence on the C31024 time spread true value than for type 8850. This is due to the fact that the C31024 photomultiplier, with optimized operating conditions, has a smaller value

of the single-photoelectron transit time spread. Comparison also shows that the C31024 time spread characteristics have a sharper knee than those of the 8850.

It can be concluded from the above considerations that, in applications where a true value of the single-photoelectron time spread is essential, the error of the measurements should be determined. This can be accomplished by an extrapolation of the data available in the transit time spread curves, such as those in Figs. 8-11.

Description of the Constant Fraction Discriminator Circuit

Timing error and resolution capabilities of the measuring system for studying photomultiplier single-electron time spread are essentially determined, in addition to the finite width of the light pulse, by the time walk and resolution characteristics of a timing discriminator. Although a number of circuits have been devised for deriving timing signals from scintillation detectors, with reduced amplitude-dependent timing error [8], our analysis and measurements have shown that the fast crossover timing with a clipping stub technique, and the constant fraction-of-pulse-height timing, based on fast tunnel-diode circuits, are the two best methods for single-photoelectron timing [15]. A modified pedestal type constant fraction discriminator

was developed with improved time walk and resolution characteristics, in which the photomultiplier signal is properly shaped by an attenuation-subtraction technique to produce a pulse with a zero-crossing point, and a pedestal added, allowing adjustment of the discriminator to the zero-crossing point. The fast baseline crossover point of a bipolar pulse is relatively independent of the pulse amplitude, and it can be conveniently used to obtain the amplitude-independent timing information. Despite the amplitude-independent crossover point of a bipolar pulse, a leading edge detector being triggered at this point introduces a time walk, in the nanosecond region, when there is a large dynamic range of input pulse amplitude. To overcome this shortcoming, a pedestal is added to shift the bias up to the detector threshold at the right time. By doing this, the detector triggers as soon as the zero-crossing point of the bipolar pulse is reached, producing an almost amplitude-independent timing pulse. To increase the input amplitude dynamic range of the discriminator, the bipolar pulse is additionally amplified and peak limited before being applied to zero-crossing and threshold detectors. All essential functions responsible for time walk in the discriminator, such as threshold discrimination and fast pulse zero crossing detection, are performed exclusively by means of tunnel diodes with backward diode

nonlinear load. Other less essential functions, such as limiting, amplification, comparison, and gating, are performed by hot carrier diodes, fast transistors, and emitter coupled logic, MECL III series.

A schematic diagram of the constant fraction discriminator is given in Fig. 12. Pertinent waveforms at the specified points in the diagram and the sequence of operation of discriminator are given in Fig. 13. Referring to both figures simultaneously, the negative unipolar input anode signal, having an amplitude anywhere from 30mV to 10V, enters the discriminator at point A, where it is split in two parts. The first part of the input signal is delayed for time t_2, by means of the delay line DL1, point B. The second part of the input signal is immediately attenuated, by a factor of 5, by means of an attenuator consisting of resistors R3 and R4, point C. The value of the resistor R1 is experimentally selected to obtain a discriminator input impedance as close as possible to 50 ohms; this reduces the value of the reflected signal from the input of the discriminator. Due to the fact that the photomultiplier, as a signal source, usually is not back-terminated, any reflected signal would be re-reflected back to the input of the discriminator. At high input signal levels, the re-reflected signal could

be high enough to be processed by the sensitive fast discriminator and the measuring system as a single-photoelectron photomultiplier signal, thus yielding spurious data. The attenuated signal is inverted by means of a wideband transformer which has a bandwidth greater than 400 MHz. The delayed and the inverted signals are added together, creating the bipolar signal at point D. An amplitude-limiting network, consisting of the hot carrier diodes CR1 and CR2, attenuates high amplitudes of the bipolar signal to a maximum of 400mV, to prevent damage and to minimize the time walk due to the overloading of the following discriminator stages. After limitation, the bipolar signal is amplified by a factor of 3 and inverted by the microwave transistor Q1. (This is indicated by the wave shape at point E.) After amplification, the bipolar signal is again amplitude limited by means of diodes CR3 and CR4.
At this point, the zero-crossover point of the bipolar signal is stable within ±15 psec through an input signal amplitude dynamic range from 50mV to 8V. This input signal amplitude dynamic range is effectively reduced to the 50mV-400mV range by the limiter-amplifier-limiter operation. The signals of the 50mV-400mV dynamic range are applied to the threshold tunnel-diode zero-crossing discriminator.

The positive portion of the bipolar pulse serves as a trigger pulse for the tunnel diode CR7 threshold detector. The peak current of the diode CR7 is 4.7mA. The fast crossover slope provides better triggering for the leading edge threshold discriminator, resulting in a pedestal with less time shift caused by wide dynamic range of the input signal pulse amplitude. Operating the leading edge threshold detector in this fashion, the pedestal time shift was found to be approximately 500 picoseconds better than the same detector triggering at the leading edge of the input signal pulse, over a dynamic range of 30:1. The variable resistor R14 is the threshold adjustment of diode CR7. Inductor L5 and the backward diode CR8 serve as the nonlinear load for tunnel diode CR7. Operating a tunnel diode in this mode improves performance in sensitivity and reduces standby power dissipation, [22]. The output of this stage in turn triggers the tunnel diode CR10, which is the pedestal generator. Diode CR10 has a peak current of 10mA. A shorting stub is the load for this stage, which generates a 25 nanosecond-long pedestal (point G). While this is taking place, the bipolar pulse is being delayed for time t_4-t_5, approximately 4 nanoseconds, by the delay cable (point F), before appearing across tunnel diode CR12, the zero-crossing detector. Diode CR12 has a peak current

of 10mA. Variable resistors R22 and R17 are for bias adjustment of the tunnel diode CR12 and the pedestal generator diode CR10, respectively. The bias pedestal is applied to the zero-crossing detector diode CR12 through inductor L7 and resistor R20. L7 is used to suppress the overshoot at the leading edge of the pedestal. Since the pedestal is used to raise the bias of CR12 nearly to its threshold level, to reduce trigger delay due to different slew rates of the zero-crossing pulses, any noise, or spike superimposed on the pedestal may trigger CR12, the zero-crossing detector, producing spurious output pulses. The zero-crossing detector is a one-shot multivibrator, using an inductor L6 and a backward diode CR11 as a nonlinear load.

The driver stage that follows uses tunnel diode CR15, inductor L8, and the backward diode CR16 as its nonlinear load. Diode CR15 has a peak current of 10mA. Variable resistor R23 provides bias adjustment for CR15.

The driver stage output signal, at the point I, is further delayed by the time t_6-t_7 of 5 nanoseconds. This is done to allow enough time for the gating signal generated by comparator M2, operating as a leading edge threshold discriminator, and the gate generator, tunnel diode CR19, to be properly applied to the reference input of comparator

M1 through the entire signal amplitude range, before the driving pulse arrives at M1. Since the comparator M2 operates in the leading edge trigger mode, the walk range of the gate signal, point M, is approximately 5 nanoseconds through a dynamic range of 35mV to 10V or 1 to 286.

In order to avoid the degradation of the time walk characteristics of the discriminator as a whole, the comparator M2 is used as the lower-level discriminator which inhibits output pulses below a certain input signal level. In this way, the threshold level of the tunnel diode CR7 is adjusted to obtain the best possible time walk characteristic throughout the entire input pulse amplitude dynamic range, and it stays fixed at that level. The variable resistor R47 is used to set the threshold level of the comparator M2 through a voltage range from 30mV to 1.6V. The output of comparator M2, point K, is differentiated by the capacitor C32 and the resistor R51. The tunnel diode CR19, normally biased at +500mV, prohibits comparator M1 from operating, since the maximum driver output signal at point J is approximately +400mV. However, with a recognized signal at the input, the negative pulse, at point L, sets CR19 to its low state of approximately +100mV. The driving signal at point J, upon exceeding the +100mV threshold level, triggers the comparator M1, yielding an output pulse at the

MECL logic levels, "0" being -1.9V, "1" being -0.8V. Transistors Q_5 and Q_6 are used to convert the signal from the MECL logic levels back to the Nuclear Instrument Module standard level, -0.8V across 50 ohms. Transistors Q_2, Q_3 and Q_4 are used to provide a positive output pulse. If necessary, the width of the positive output pulse can be lengthened by using a pulse standardizer or a retriggerable one shot multivibrator.

Time Walk and Resolution Characteristics of the Constant Fraction Discriminator

The time walk and resolution characteristics of the constant fraction discriminator, as a function of the input pulse amplitude, were measured with the input pulse rise time and width as parameters. Measurements were made using the system described in reference [15]. Essentially, the source of the discriminator input pulses was a fast rise time pulse generator, combined with the integrator when pulses with different rise times were necessary. The triggering signal from the pulse generator was applied to the external trigger terminal of a two channel sampling oscilloscope. The output pulses from the pulse generator (or integrator) were applied to the constant fraction discriminator via an 18 GHz attenuator, which has a negligible time walk for different attenuation settings. Also, a part of the same generator output pulse was applied as a reference timing signal to one channel of the sampling

oscilloscope via a pick off probe and a delay line. The output signal from the constant fraction discriminator was applied to the other channel of the oscilloscope. The time walk characteristics of the discriminator were then found by comparing the 50% point of the amplitude of the leading edge of the reference pulse and the 50% point of the amplitude of the leading edge of the discriminator output pulse. Using the 20 db attenuator setting as a reference point, the time-walk characteristics of the discriminator were measured. The characteristics are shown in Fig. 14. The time-walk of the discriminator, at a repetition frequency of 100 KHz, in the best possible case has a value from -35 psec to +35 psec for an input pulse amplitude variation from 35mV to 8V, and an input pulse rise time and width of t_r = 2.5 nsec, and t_w = 10 nsec, respectively. The time walk is from -55 psec to +55 psec for the same input pulse amplitude variations as in the previous case, where the input pulse rise time and width are t_r = 0.8 nsec and t_w = 2 nsec, respectively.

The discriminator time resolution was also measured, as a function of the input pulse amplitude, with the input pulse rise time and width as parameters, by means of the measuring system described in Ref. [15]. The measured time resolution of the system without the constant fraction discriminator was 15 psec FWHM. Results of the measurements are given in Fig. 15. It can be seen that the total system

time resolution, including the constant fraction discriminator, is 20 psec FWHM for an input pulse amplitude variation from 300mV to 8V and for a pulse rise time and width of 0.8 nsec and 2 nsec, respectively. The time resolution is 78 psec and 130 psec for input rise times of 0.8 nsec and 2.5 nsec, respectively. In general, the total time resolution is practically determined at low values of input pulse amplitude by the time resolution of the constant fraction discriminator.

Conclusions

Single-photoelectron transit time spread and relative collection efficiency measurements of fast photomultipliers, having dynodes with cesium-activated gallium-phosphide secondary emitting surfaces, have been presented and discussed. For the RCA 8850 photomultiplier, measurements were made using the voltage divider network suggested by the photomultiplier manufacturer, with operating voltages of 2000V, 2500V, and 3000V. Measurements of transit time spread of the C31024 were made using a modified voltage divider that establishes a photocathode-first dynode voltage of 1100V. A description of the measuring system and measuring techniques was given in detail. Furthermore, a determination of photomultiplier optimum operating conditions, with regard to the single-photoelectron transit time

spread and the relative collection efficiency, showed that optimization for minimum time spread can be accomplished without a significant reduction of the collection efficiency.

Influences of the finite width of the light pulse, and the time walk and resolution characteristics of the timing discriminator, on the timing error and resolution capabilities of the measuring system have been investigated. Measurements of the dependence of the time spread on light pulses of different width have been presented in detail and discussed. Finally, a new subnanosecond constant fraction discriminator has been developed with better time walk and resolution characteristics than previously available. The discriminator has been employed in the improved measuring system with increased time resolution capabilities. The system and its critical individual devices can be easily modified for applications in a number of practical cases where very high time resolution in the subnanosecond region is required.

Acknowledgment

This work was performed as part of the program of the Electronics Research and Development Group of the Lawrence Berkeley Laboratory, University of California, Berkeley, and was supported by the U. S. Atomic Energy Commission, Contract No. W-7405-eng-48.

References

[1] F. A. White, Mass Spectrometry in Science and Technology, Wiley, New York (1968).

[2] J. B. Birks, The Theory and Practice of Scintillation Counting, Pergamon Press, New York (1964).

[3] J. Yguerabide, Nanosecond Fluorescence Spectroscopy of Macromolecules, Methods in Enzymology, Vol. XXVI, Enzyme Structure, Part C, edited by C. H. W. Hirs, S. N. Timasheff, pp. 498-578, Academic Press, New York (1972).

[4] W. Meiling, F. Stary, Nanosecond Pulse Technique, Gordon & Breach, New York (1968).

[5] S. Poultney, Single Photon Detection and Timing in the Lunar Laser Ranging Experiment. IEEE Transactions on Nuclear Science, NS-19, No. 3, pp. 12-17 (1972).

[6] H. Melchior, M. B. Fisher, F. R. Arams, Photodetectors for Optical Communication Systems, Proceedings of the IEEE, Vol. 58, No. 10, pp. 1466-1486, October 1970.

[7] E. Pike, Photon Statistics, Quantum Optics, S. M. Kay and A. Maitland, eds., Academic Press, New York, pp. 127-176, (1970).

[8] Sherman K. Poultney, Single Photon Detection and Timing: Experiments and Technique, Advances in Electronics and Electron Physics, 31, Marton, ed., 39-117 (1972).

[9] C. R. Kerns, Photomultiplier Single-Electron Time-Spread Measurements, IEEE Transactions on Nuclear Science, NS-14, No. 1, pp. 449-454 (1967).

[10] G. Present and D. B. Searl, Single-Photon Time Resolution of Photomultipliers with Gallium Phosphide First Dynode, Review of Scientific Instruments, 41, pp. 771-772 (1970).

[11] C. C. Lo, B. Leskovar, Evaluation of the 8850 Photomultiplier with a Cesiated Gallium-Phosphide First Dynode, Engineering Note No. 1383, September 1971, Lawrence Berkeley Laboratory, Berkeley, California.

[12] C. C. Lo, B. Leskovar, Evaluation of the C30133B Photomultiplier with a Cesiated Gallium-Phosphide First Dynode, Engineering Note No. 1387, October 1971, Lawrence Berkeley Laboratory, Berkeley, California.

[13] C. C. Lo, B. Leskovar, Preliminary Results of Tests of the C31024 High Speed Photomultiplier with Cesiated Gallium-Phosphide Dynodes, Engineering Note No. 1384, October 1971, Lawrence Berkeley Laboratory, Berkeley, California.

[14] B. Leskovar, C. C. Lo, Performance Studies of Photomultipliers Having Dynodes with GaP(Cs) Secondary Emitting Surface, IEEE Transactions on Nuclear Science, NS-19, No. 3, pp. 60-72 (1972).

[15] C. C. Lo, B. Leskovar, A Measuring System for Studying the Time-Resolution Capabilities of Fast Photomultipliers, IEEE Transactions on Nuclear Science, NS-21, No. 1, pp. 93-105 (1974).

[16] G. Pietri, Progress in PMT for High Energy Physics Instrumentation, 1973 Internation Conference on Instrumentation for High Energy Physics, Ed. S. Stipcich, pp. 586-591, (September 1973).

[17] L. K. Anderson, M. DiDomenico, Jr., High Speed Photodetectors for Microwave Demodulation of Light in Advances in Microwaves, L. Young, ed., Vol. 5, pp. 1-121 (1970).

[18] R. E. Simon, B. F. Williams, Secondary-Electron Emission, IEEE Transactions on Nuclear Science, NS-15, No. 3, pp. 167-170 (1968).

[19] G. A. Morton, H. M. Smith, H. R. Krall, The Performance of High-Gain First-Dynode Photomultipliers, IEEE Transactions on Nuclear Science, NS-16, pp. 92-95 (1969).

[20] H. R. Krall, F. A. Helvy, D. E. Persyk, Recent Developments in GaP(Cs) Dynode Photomultipliers, IEEE Transactions on Nuclear Science, NS-17, No. 3, pp. 71-74 (1970).

[21] H. R. Krall, D. E. Persyk, Recent Work on Fast Photomultiplier Utilizing GaP(Cs) Dynodes, IEEE Transactions on Nuclear Science, NS-19, No. 3, pp. 45-59 (1972).

[22] S. L. Sarnot, "On the Use of a Nonlinear Element in Tunnel Diode Circuits," Proceedings of the IEEE, 59, No. 1, pp. 107-108, January 1971.

[23] B. Fan, B. Leskovar, C. C. Lo, G. A. Morton, T. K. Gustafson, A High-Repetion-Rate Nd:Glass Laser Mode-Locked by a Saturable Absorber. It will be published in the IEEE Journal of Quantum Electronics, September 1974.

[24] B. Fan, B. Leskovar, C. C. Lo, G. A. Morton, T. K. Gustafson, High Repetition Rate Picosecond Neodymium-Glass Laser, Engineering Note No. 1414, April 1974, Lawrence Berkeley Laboratory, Berkeley, California.

Figure Captions

Fig. 1. Block diagram of the system for measuring the single-photoelectron time spread of fast photomultipliers.

Fig. 2. Single-electron time spread and relative collection efficiency, as a function of the voltage ratio between the photocathode-focusing electrode and photocathode-first dynode for the RCA 8850 photomultiplier with a 1.6 mm-diameter area of photocathode illumination.

Fig. 3. Single-electron time spread and relative collection efficiency, as a function of the voltage ratio between the photocathode-focusing electrode and the photocathode-first dynode for the RCA 8850 photomultiplier with full photocathode illumination.

Fig. 4. Single-electron time spread of the RCA 8850 photomultiplier with a 1.6 mm-diameter area of photocathode illumination.

Fig. 5. Single-electron time spread and relative collection efficiency as a function of the voltage ratio between the photocathode-focusing electrode and photocathode-first dynode for the RCA C31024 photomultiplier with a 1.6 mm-diameter area of photocathode illumination.

Fig. 6. Single-electron time spread and relative collection efficiency, as a function of the voltage ratio between the photocathode-focusing electrode and photocathode-first dynode for the RCA C31024 photomultiplier with full photocathode illumination.

Fig. 7. Single-electron time spread of the RCA C31024 photomultiplier with a 1.6 mm-diameter area of photocathode illumination.

Fig. 8. Single-electron time spread of RCA 8850 as a function of the width of the electroluminescent diode current pulse for 1.6 mm-diameter area of photocathode illumination, with supply voltage between the anode and cathode as the parameter.

Fig. 9. Single-electron time spread of RCA 8850 as a function of the width of the electroluminescent diode current pulse for full photocathode illumination, with supply voltage between anode and cathode as the parameter.

Fig. 10. Single-electron time spread of the RCA C31024 as a function of the width of the electroluminescent diode current pulse for the 1.6 mm-diameter area of photocathode illumination, with supply voltage between anode and cathode as the parameter.

Fig. 11. Single-electron time spread of the RCA C31024 as a function of the width of the electroluminescent diode current pulse for full photocathode illumination, with voltage ratio between the photocathode-focusing electrode and photocathode-first dynode as the parameter.

Fig. 12. Schematic diagram of the constant fraction discriminator.

Fig. 13. Waveforms at the particular points in the constant fraction discriminator schematic diagram of Fig. 12.

Fig. 14. Time-walk characteristics of the constant fraction discriminator as a function of the amplitude of the input pulse, with input pulse rise time and width as parameters.

Fig. 15. Discriminator time-resolution characteristics as a function of the input pulse amplitude, with input pulse rise time and width as parameters.

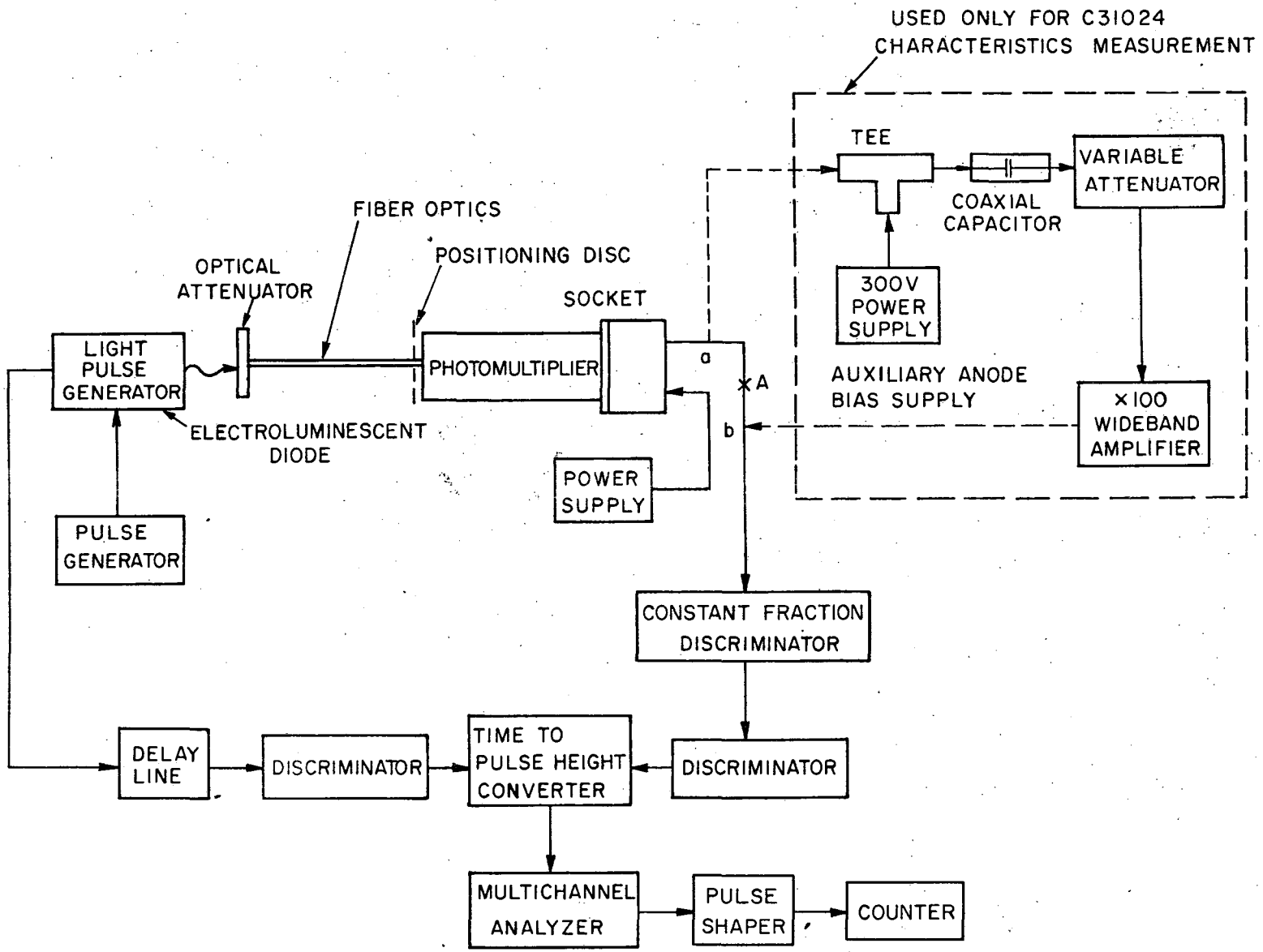
USED ONLY FOR C31024
CHARACTERISTICS MEASUREMENT
TEE
VARIABLE ATTENUATOR
COAXIAL CAPACITOR
300V POWER SUPPLY
FIBER OPTICS
POSITIONING DISC
OPTICAL ATTENUATOR
SOCKET
LIGHT PULSE GENERATOR
PHOTOMULTIPLIER
a
A
b
AUXILIARY ANODE BIAS SUPPLY
×100 WIDEBAND AMPLIFIER
ELECTROLUMINESCENT DIODE
POWER SUPPLY
PULSE GENERATOR
CONSTANT FRACTION DISCRIMINATOR
DELAY LINE
DISCRIMINATOR
TIME TO PULSE HEIGHT CONVERTER
DISCRIMINATOR
MULTICHANNEL ANALYZER
PULSE SHAPER
COUNTER
XBL 746-1042

Fig. 1

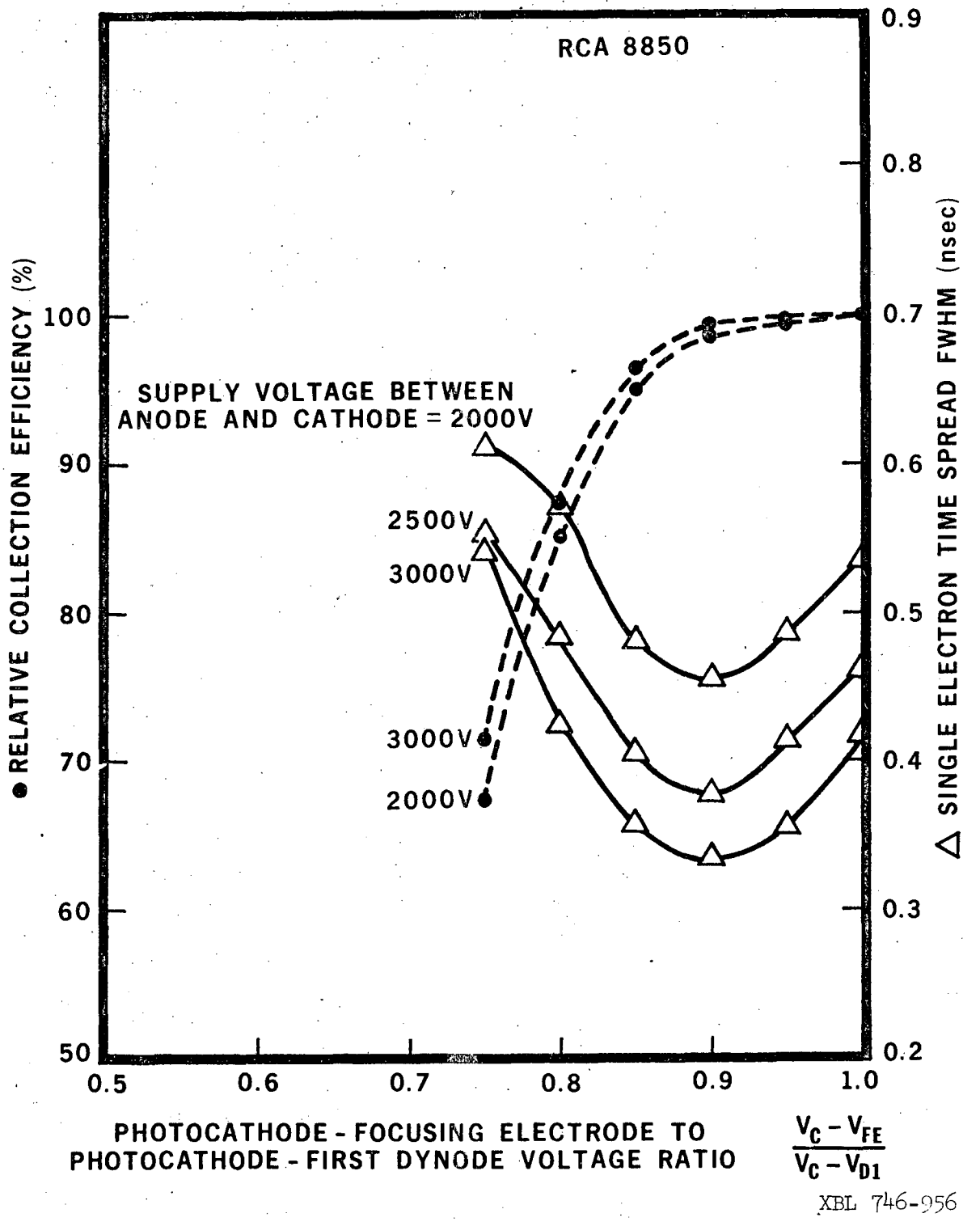
RCA 8850
SUPPLY VOLTAGE BETWEEN
ANODE AND CATHODE = 2000V
2500V
3000V
3000V
2000V
● RELATIVE COLLECTION EFFICIENCY (%)
△ SINGLE ELECTRON TIME SPREAD FWHM (nsec)
100
90
80
70
60
50
0.9
0.8
0.7
0.6
0.5
0.4
0.3
0.2
0.5
0.6
0.7
0.8
0.9
1.0
PHOTOCATHODE - FOCUSING ELECTRODE TO
PHOTOCATHODE - FIRST DYNODE VOLTAGE RATIO
$\frac{V_C - V_{FE}}{V_C - V_{D1}}$
XBL 746-956

Fig. 2

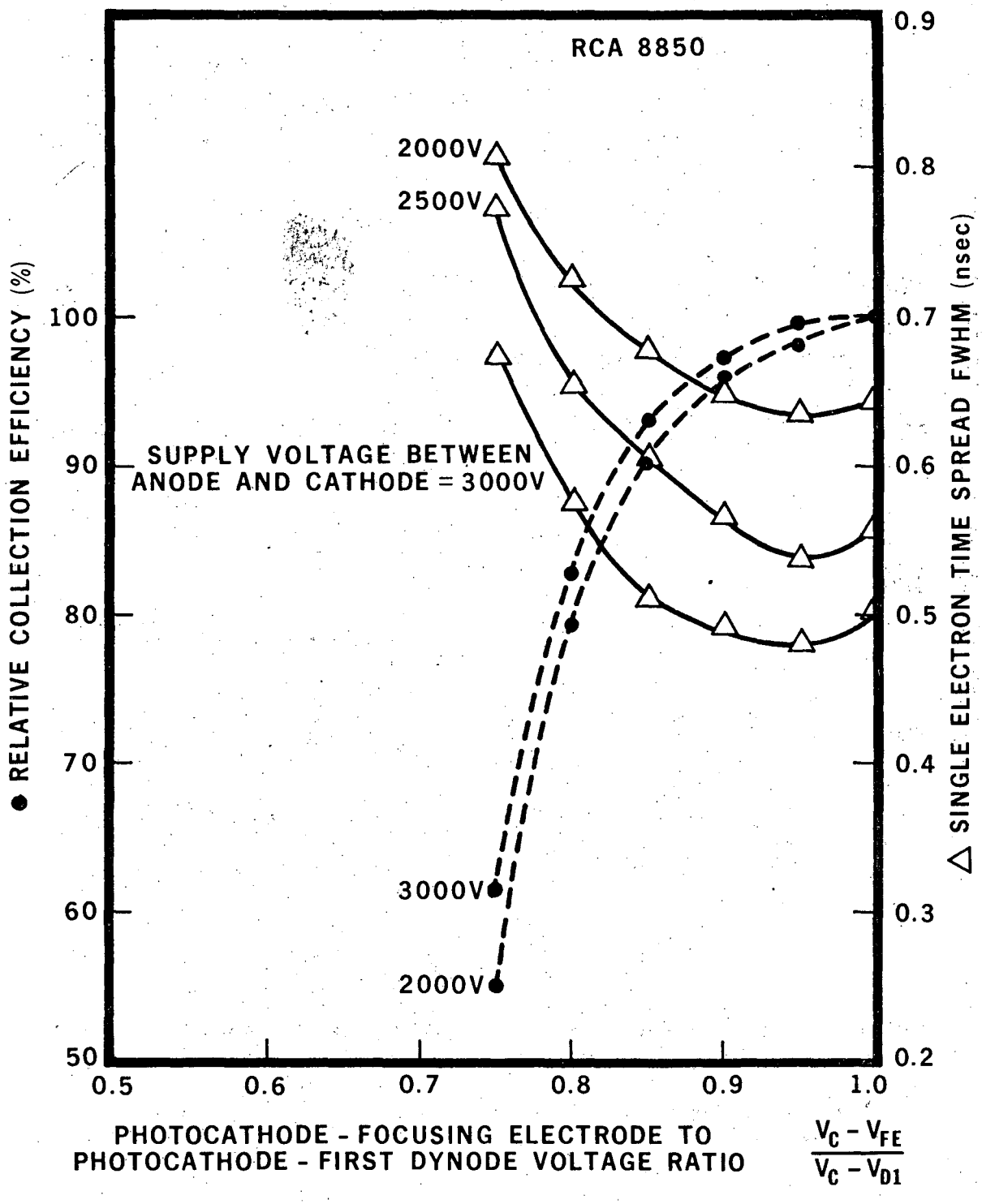
RCA 8850
2000V
2500V
3000V
2000V
SUPPLY VOLTAGE BETWEEN
ANODE AND CATHODE = 3000V
● RELATIVE COLLECTION EFFICIENCY (%)
△ SINGLE ELECTRON TIME SPREAD FWHM (nsec)
100
90
80
70
60
50
0.9
0.8
0.7
0.6
0.5
0.4
0.3
0.2
0.5
0.6
0.7
0.8
0.9
1.0
PHOTOCATHODE - FOCUSING ELECTRODE TO
PHOTOCATHODE - FIRST DYNODE VOLTAGE RATIO
$\frac{V_C - V_{FE}}{V_C - V_{D1}}$
XBL 746-954

Fig. 3

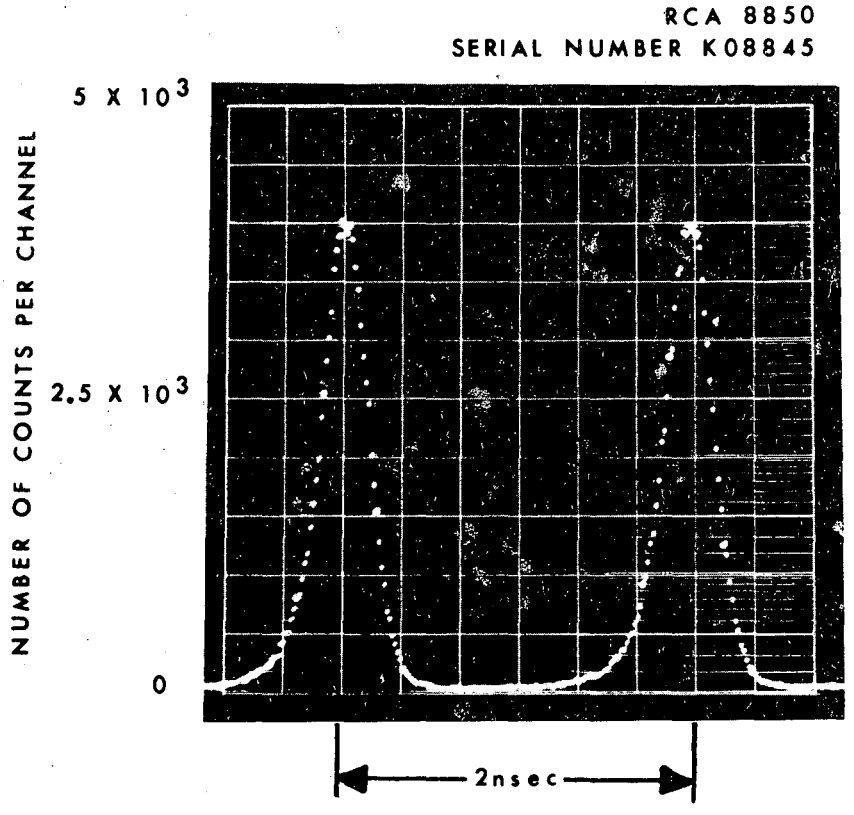

CALIBRATION = 15.5psec PER CHANNEL
SINGLE ELECTRON TIME SPREAD FWHM = 330psec
SUPPLY VOLTAGE BETWEEN ANODE AND CATHODE = 3000V

$$\frac{V_C - V_{FE}}{V_C - V_{D1}} = 0.9$$

XBB 746-4049

Fig. 4

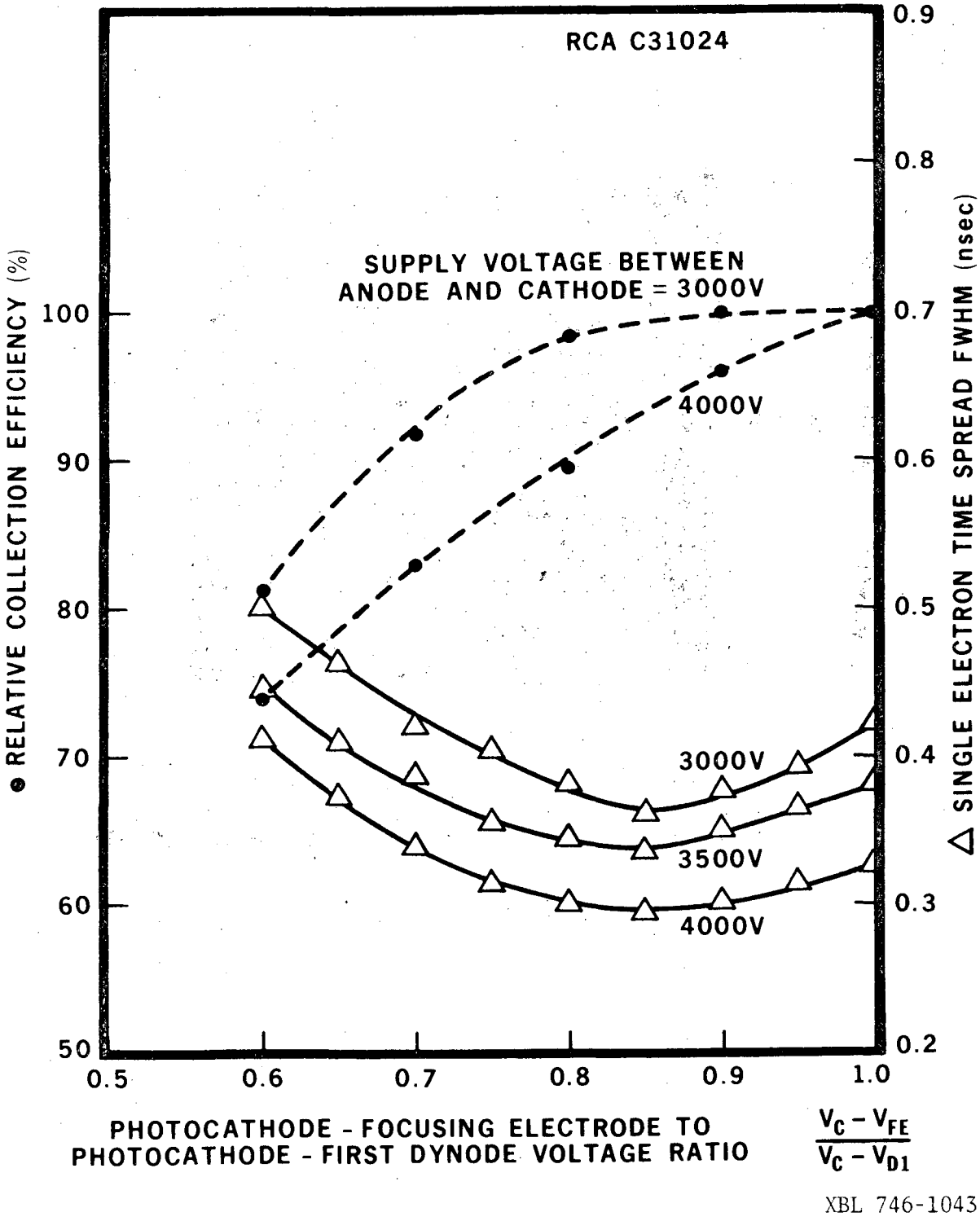

XBL 746-1043

Fig. 5

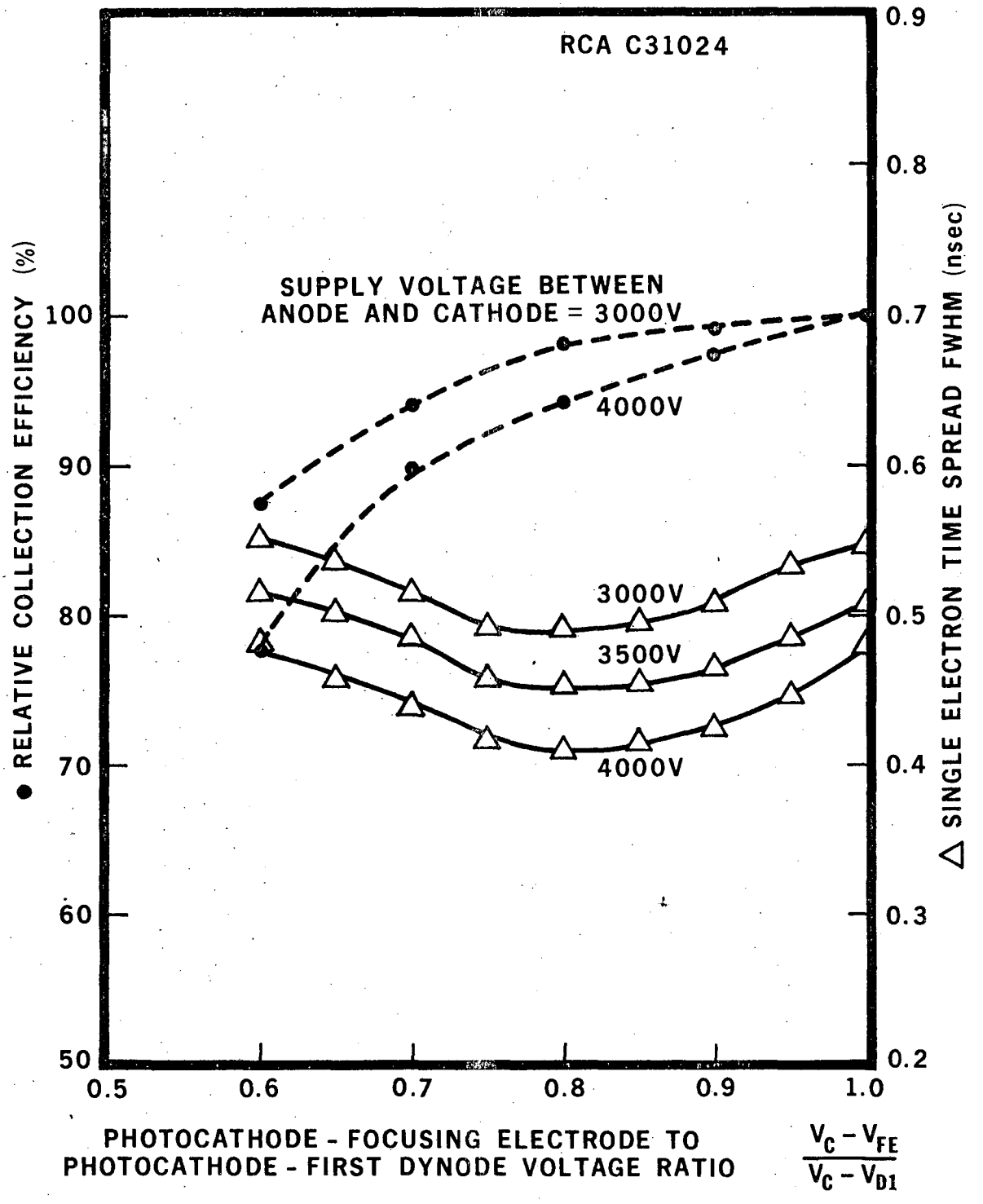

XBL 746-1044

Fig. 6

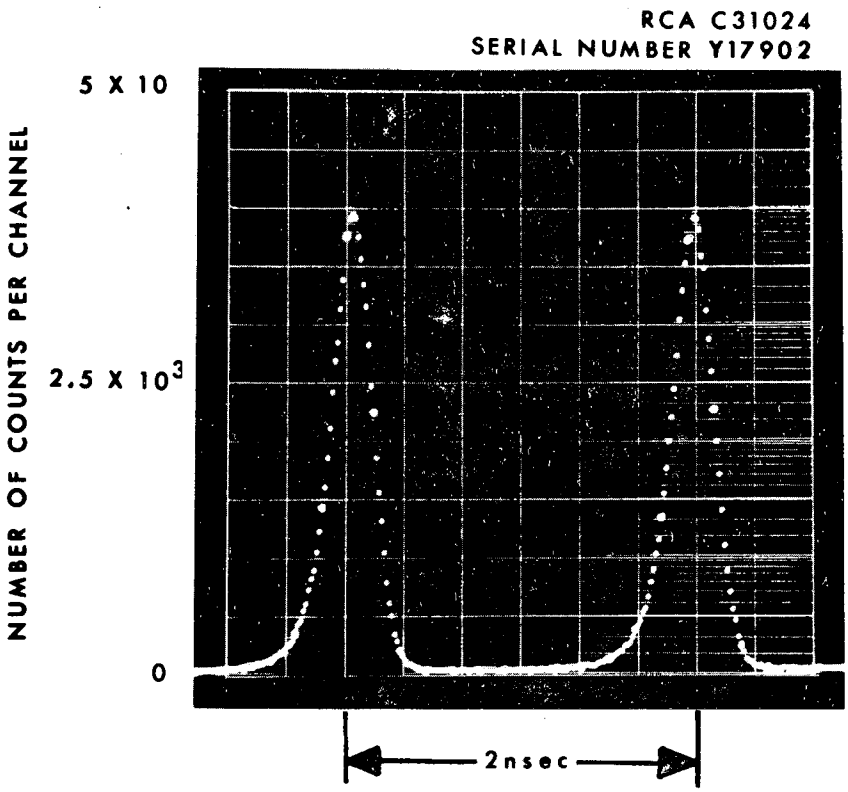

CALIBRATION = 15.5psec PER CHANNEL
SINGLE ELECTRON TIME SPREAD FWHM = 270psec
SUPPLY VOLTAGE BETWEEN ANODE AND CATHODE = 4000V

$$V_C - V_{D1} = 1100V$$

$$\frac{V_C - V_{FE}}{V_C - V_{D1}} = 0.9$$

XBB 746-4048

Fig. 7

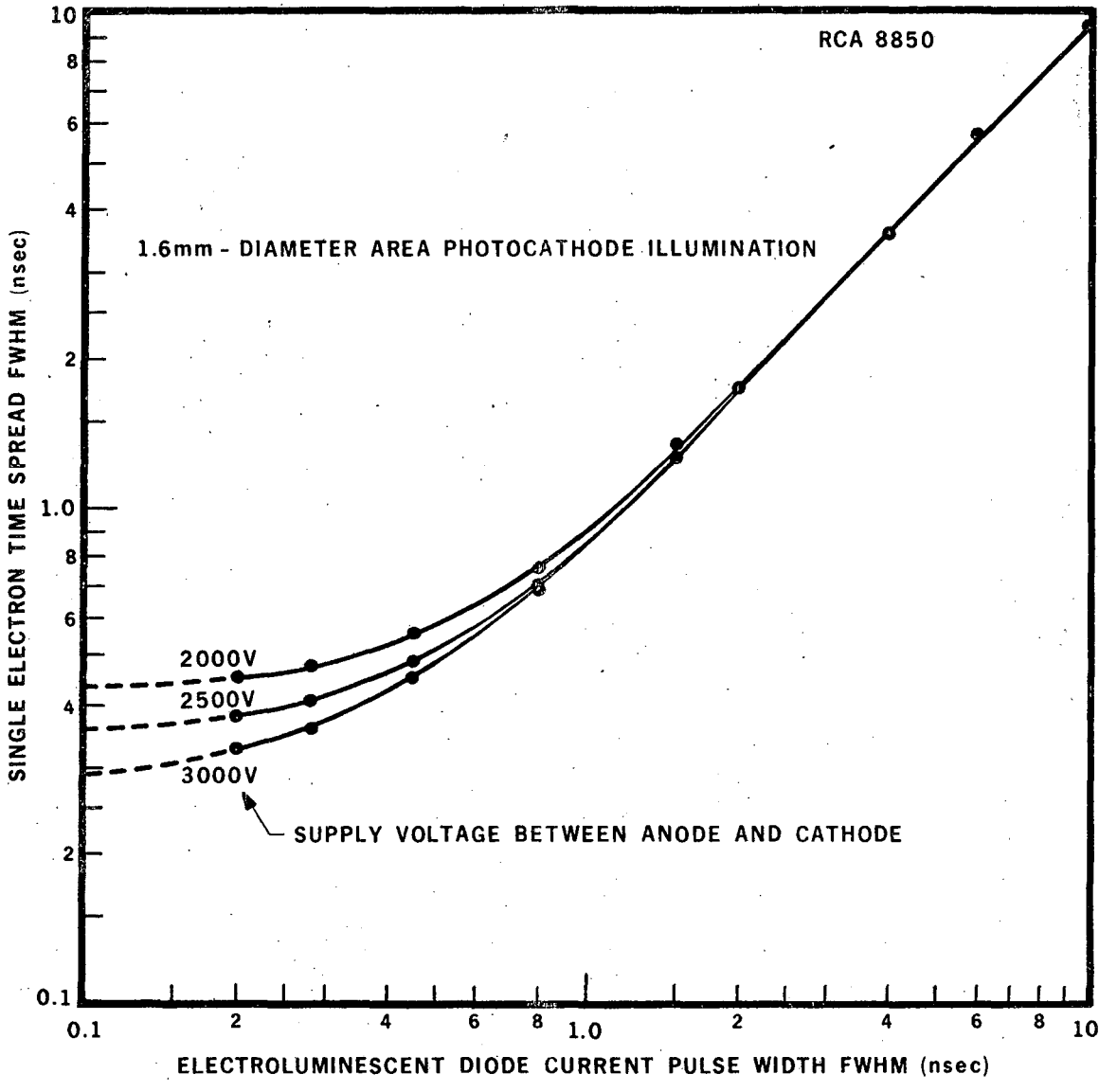

XBL 746-977

Fig. 8

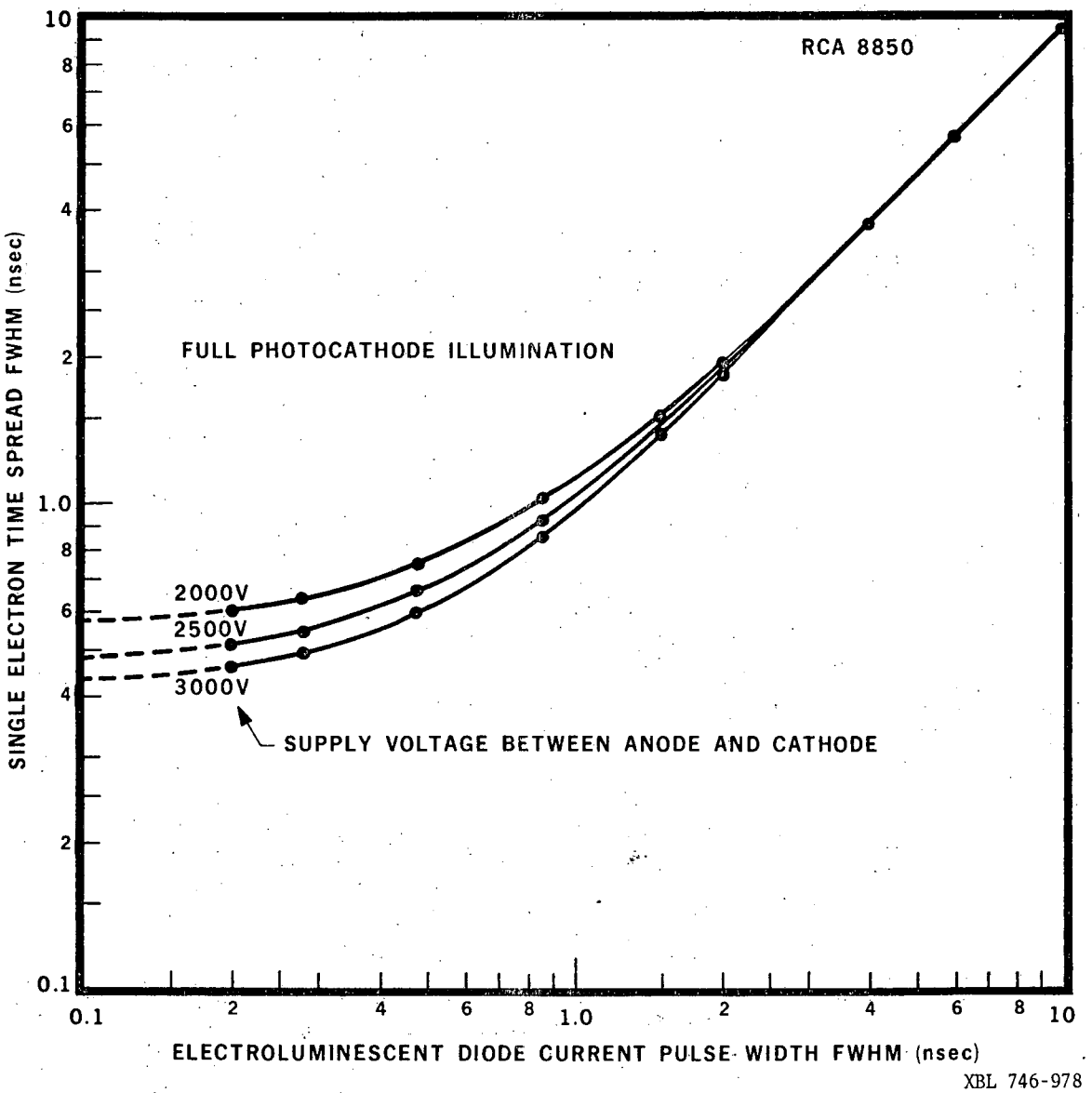
RCA 8850
FULL PHOTOCATHODE ILLUMINATION
2000V
2500V
3000V
SUPPLY VOLTAGE BETWEEN ANODE AND CATHODE
SINGLE ELECTRON TIME SPREAD FWHM (nsec)
ELECTROLUMINESCENT DIODE CURRENT PULSE WIDTH FWHM (nsec)
10
8
6
4
2
1.0
8
6
4
2
0.1
0.1
2
4
6
8
1.0
2
4
6
8
10
XBL 746-978

Fig. 9

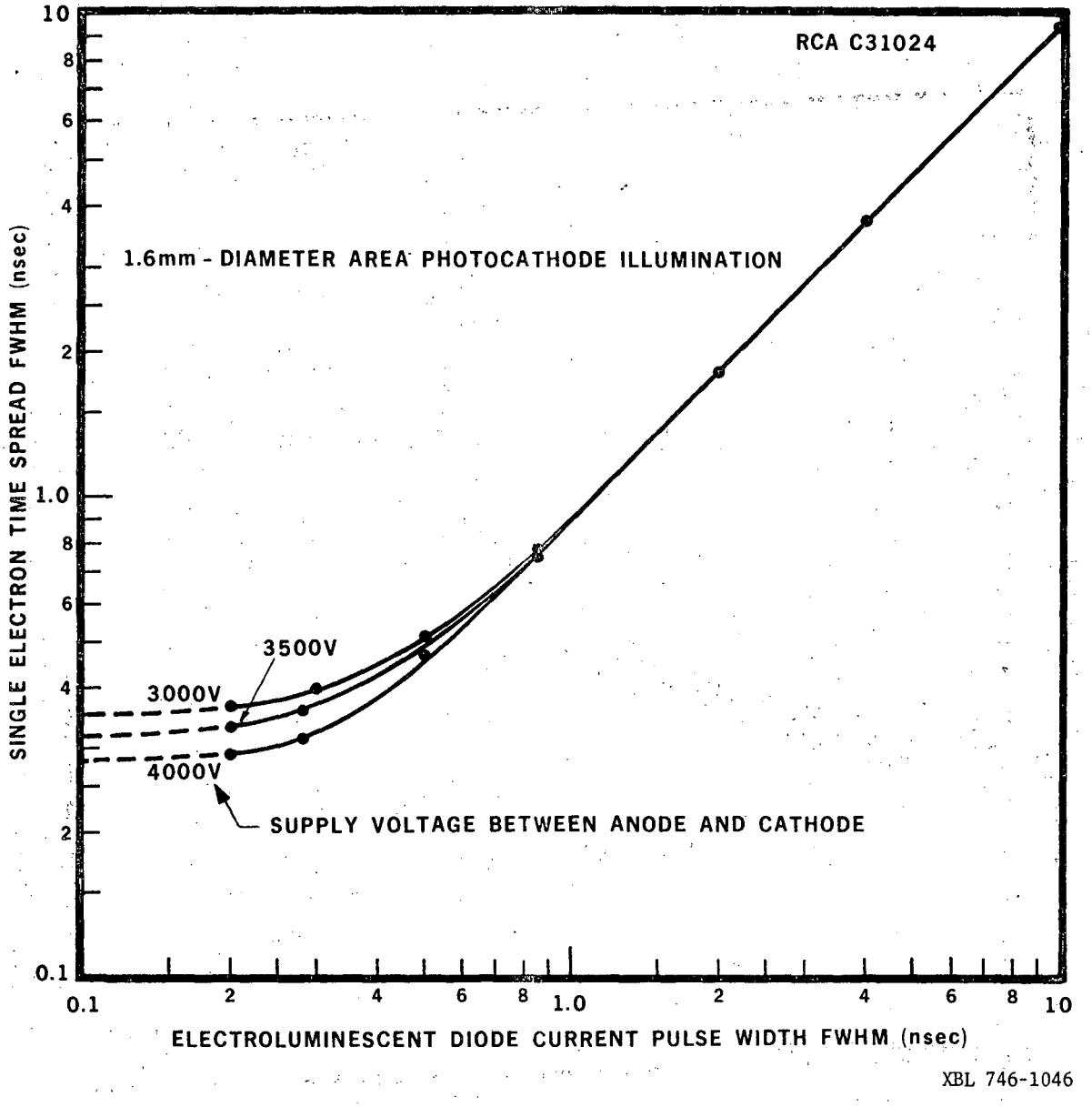
RCA C31024
1.6mm - DIAMETER AREA PHOTOCATHODE ILLUMINATION
3500V
3000V
4000V
SUPPLY VOLTAGE BETWEEN ANODE AND CATHODE
SINGLE ELECTRON TIME SPREAD FWHM (nsec)
ELECTROLUMINESCENT DIODE CURRENT PULSE WIDTH FWHM (nsec)
10
8
6
4
2
1.0
8
6
4
2
0.1
0.1
2
4
6
8
1.0
2
4
6
8
10
XBL 746-1046

Fig. 10

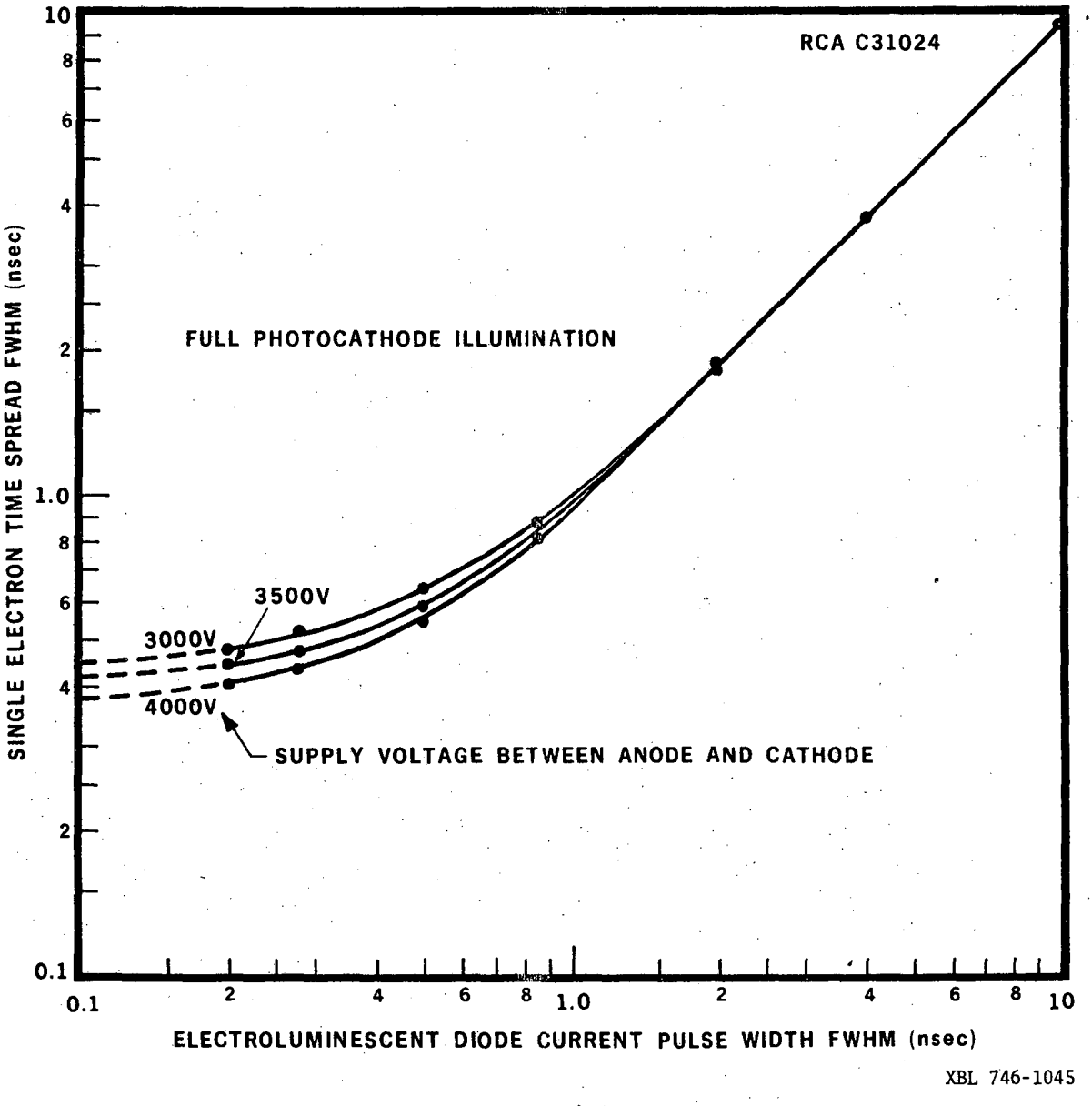
RCA C31024
FULL PHOTOCATHODE ILLUMINATION
3500V
3000V
4000V
SUPPLY VOLTAGE BETWEEN ANODE AND CATHODE
SINGLE ELECTRON TIME SPREAD FWHM (nsec)
ELECTROLUMINESCENT DIODE CURRENT PULSE WIDTH FWHM (nsec)
10
8
6
4
2
1.0
8
6
4
2
0.1
0.1
2
4
6
8
1.0
2
4
6
8
10
XBL 746-1045

Fig. 11

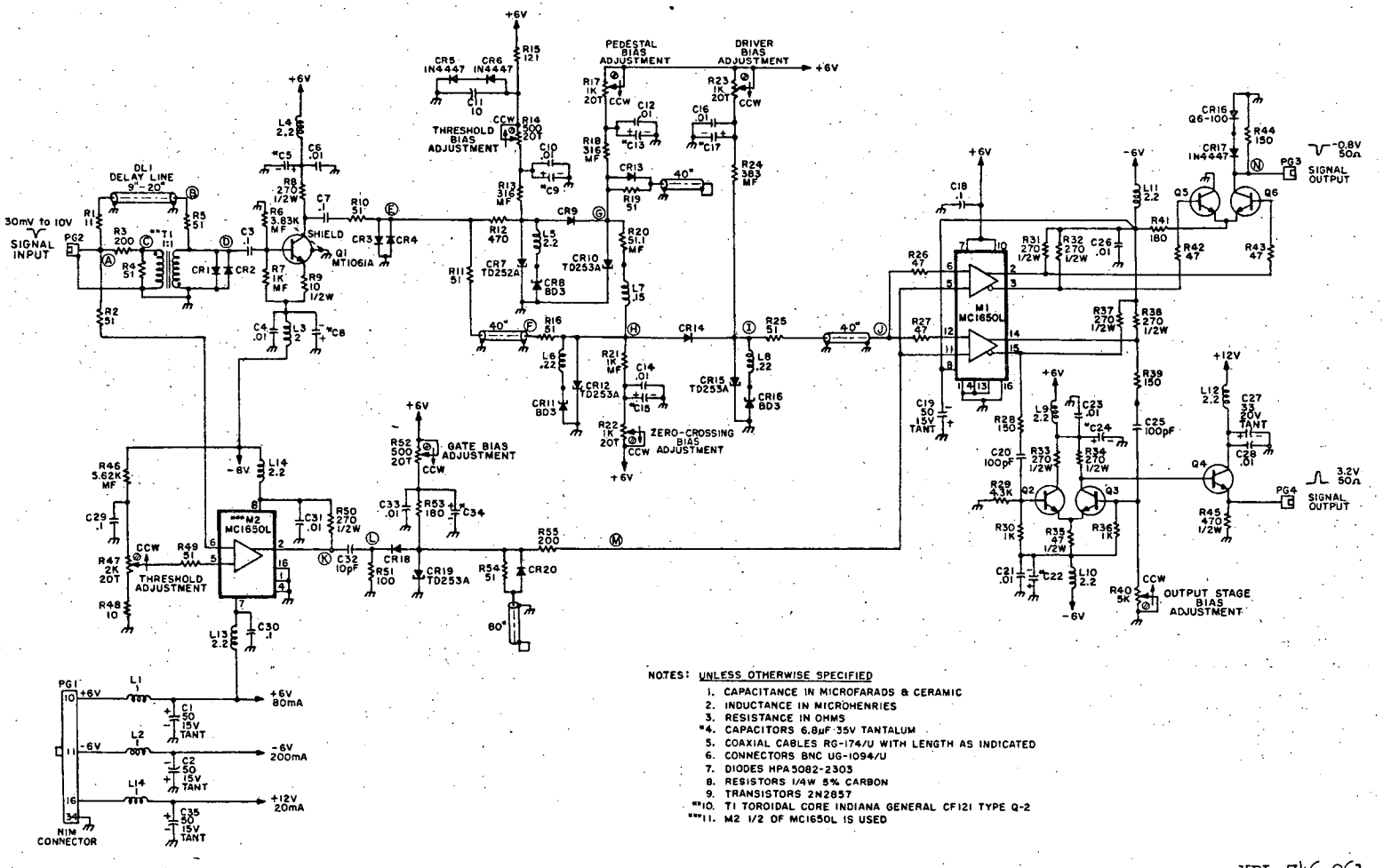

NOTES: UNLESS OTHERWISE SPECIFIED

1. CAPACITANCE IN MICROFARADS & CERAMIC
2. INDUCTANCE IN MICROHENRIES
3. RESISTANCE IN OHMS
*4. CAPACITORS 6.8μF 35V TANTALUM
5. COAXIAL CABLES RG-174/U WITH LENGTH AS INDICATED
6. CONNECTORS BNC UG-1094/U
7. DIODES HPA3082-2303
8. RESISTORS 1/4W 5% CARBON
9. TRANSISTORS 2N2857
**10. T1 TOROIDAL CORE INDIANA GENERAL CF121 TYPE Q-2
***11. M2 1/2 OF MC1650L IS USED

XBL 746-961

Fig. 12

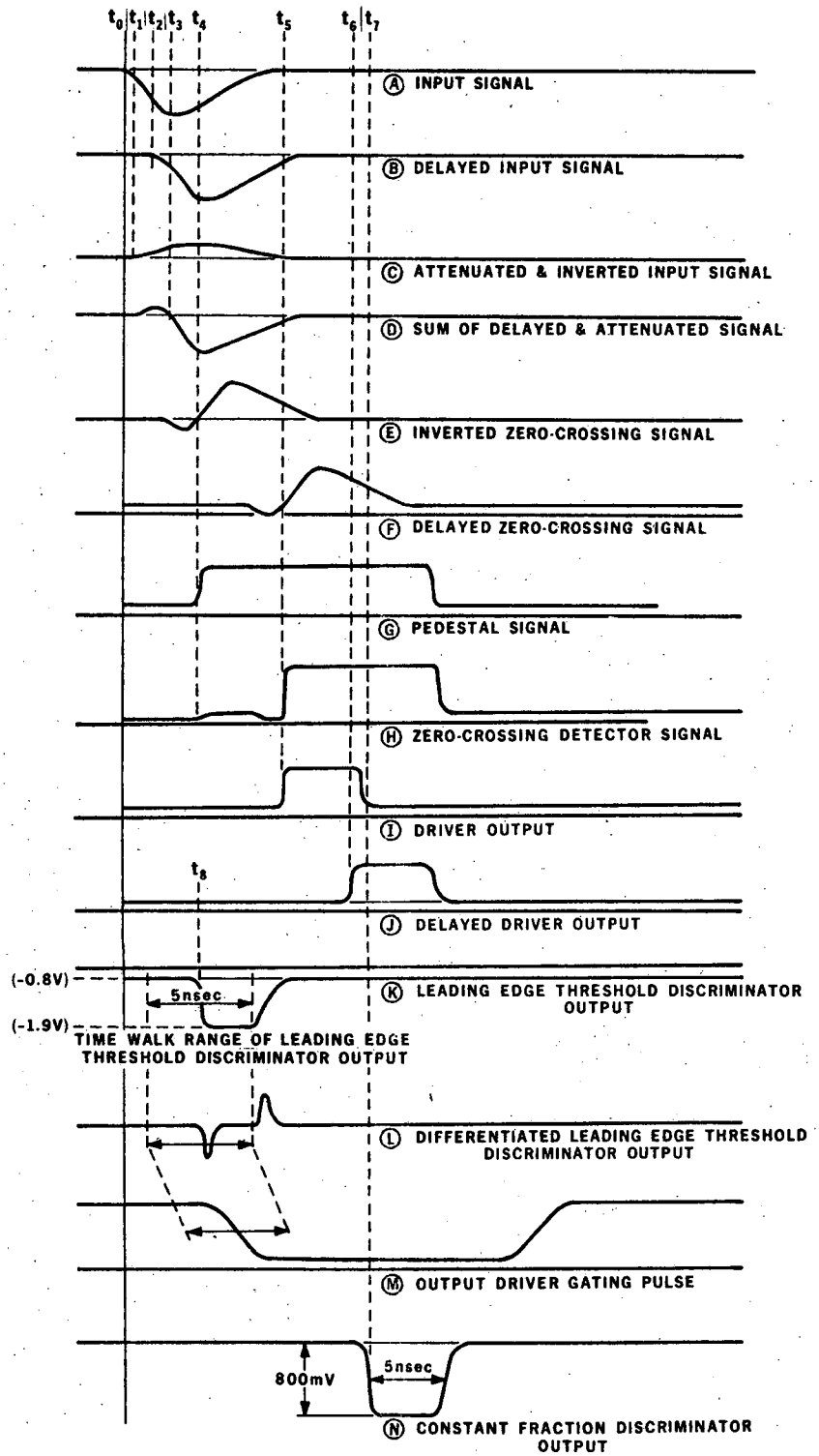

XBL 746-960

Fig. 13

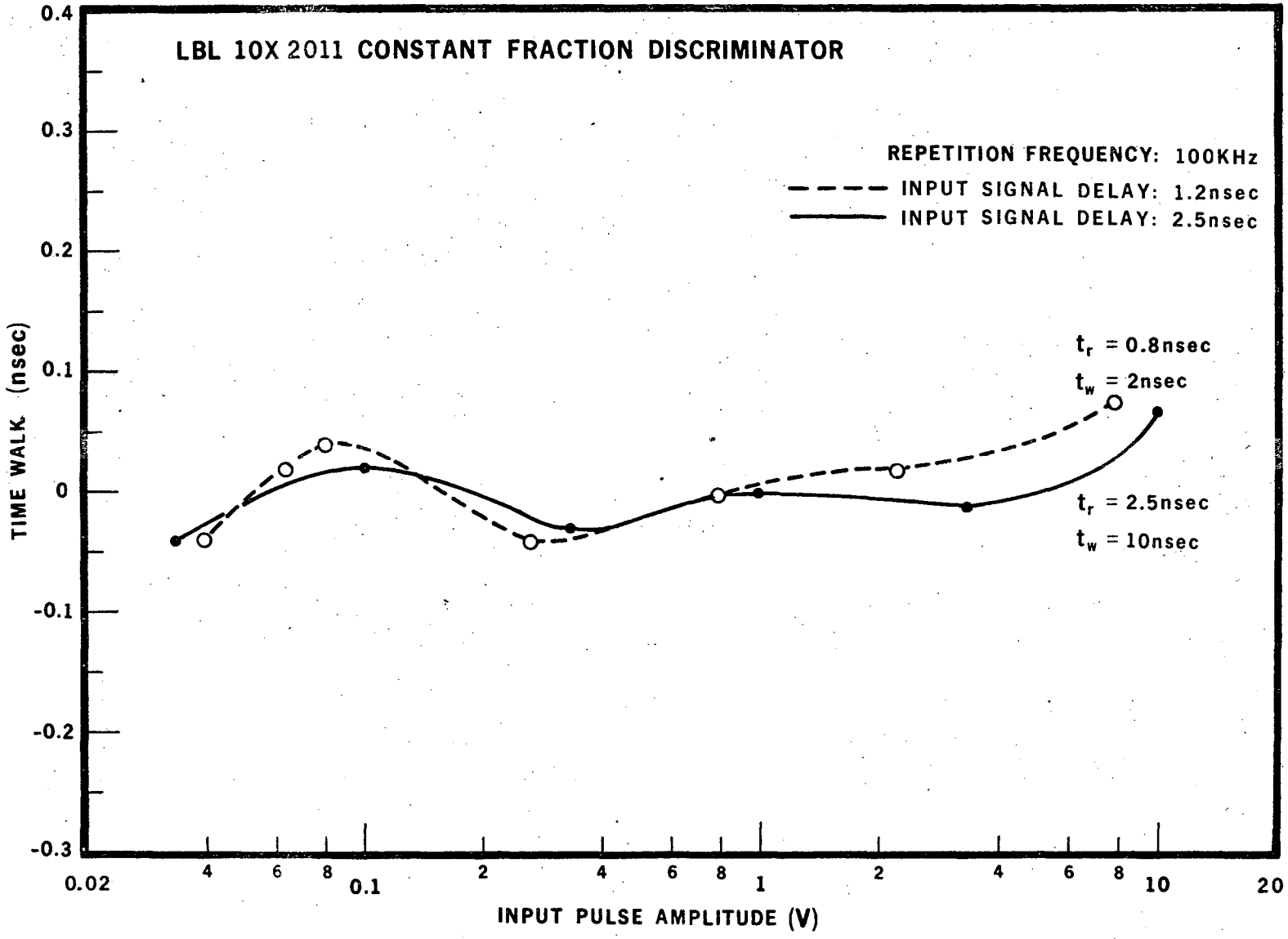

XBL 746-958

Fig. 14

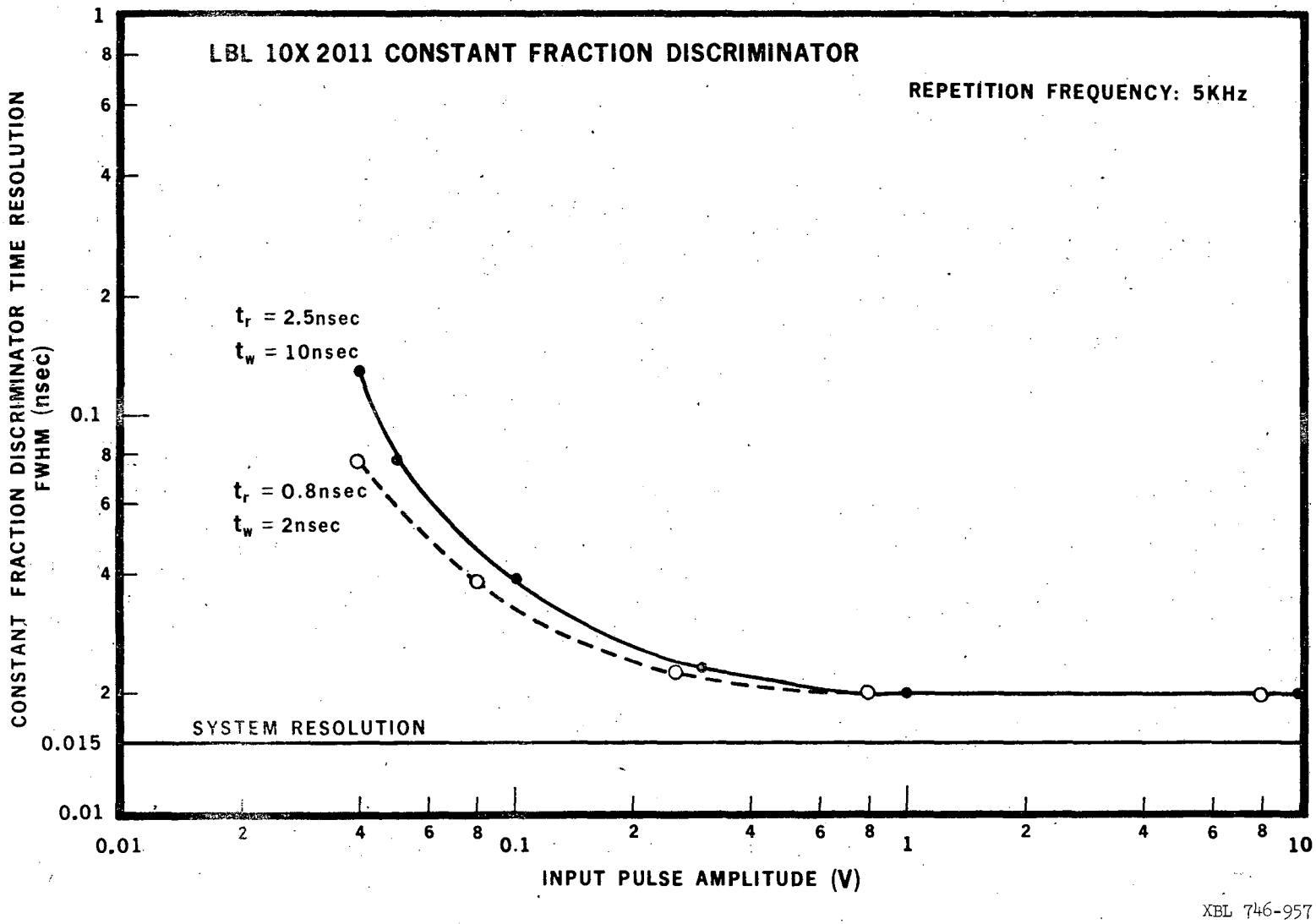

XBL 746-957

Fig. 15

TECHNICAL INFORMATION DIVISION
LAWRENCE BERKELEY LABORATORY
UNIVERSITY OF CALIFORNIA
BERKELEY, CALIFORNIA 94720